On the retardation mechanisms of citric acid in ettringite-based binders

Hoang Nguyen [a,*], Wolfgang Kunther [b], Katrijn Gijbels [c], Pieter Samyn [d], Valter Carvelli [e], Mirja Illikainen [a], Paivo Kinnunen [a]

[a] *Fibre and Particle Engineering Research Unit, University of Oulu, Pentti Kaiteran katu 1, 90014 Oulu, Finland*
[b] *Department of Civil Engineering, Technical University of Denmark, 2800 Kgs. Lyngby, Denmark*
[c] *Nuclear Technological Centre, Hasselt University, Agoralaan, Gebouw H, 3590 Diepenbeek, Belgium*
[d] *IMO, Applied and Analytical Chemistry, Hasselt University, Agoralaan, Gebouw D, 3590 Diepenbeek, Belgium*
[e] *Department A.B.C., Politecnico di Milano, Piazza Leonardo Da Vinci 32, 20133 Milan, Italy*

ARTICLE INFO

ABSTRACT

This study aims to obtain insights into the retardation mechanism of citric acid in an ettringite-based binder from ladle slag and gypsum. The hydration kinetics and phase assemblage of the binder were experimentally investigated and thermodynamically modelled. Additionally, the effects of citric acid on synthetic ettringite were studied to obtain further understanding of the interaction between this organic ligand and the crystal. Experimental results reveal that citric acid works as an inhibitor of ettringite's formation leading to the precipitation of monosulfate and gypsum; the ettringite surface blockage by citrate ligand effectively prevents precipitation of this crystal. This leads to an overestimation in the precipitation of ettringite in the thermodynamic model due to this kinetic barrier imposed by the ligand. Thermodynamic modelling suggests ettringite, monosulfate, aluminum hydroxide, and strätlingite as main hydrates in this binder, whereas an intermixed C–(A–)S–H gel was observed experimentally instead of strätlingite.

1. Introduction

The development of alternative cementitious binders, beside conventional Portland cement, is seen as a path to a more sustainable construction industry in the future, as the efficient use of industrial by-products will lower the environmental impact of cement manufacturing process [1]. However, each new binder development comes with the need to obtain understanding of the hydration mechanism, kinetics, and the resulting phase assemblages of the developed alternative binders and their engineering properties. Additives, such as set retarders, are often used in small dosages. However, they can alter the binder's hydration process, possibly affect the hydration products, and eventually the binder's performance. Insights into these topics are needed to establish the state of technology that allows the implementation in standards and design codes, and the use on construction sites or precast plants.

Thermodynamic modelling has been recognized as an efficient tool to provide understanding of the of hydration mechanisms in different cementitious systems [2–4]. Currently, thermodynamic databases for cement research [5] allow for the thermodynamic modelling of the most common cementitious binders and their phase evolution when kinetic models are utilized [6–8]. However, thermodynamic modelling cannot predict phases that are not included in its database or cannot derive the kinetics of processes ab initio reliably. The modelling for the influences of organic admixtures and additives on cementitious binders can fall in both aforementioned issues, and therefore, only few publications on the modelling of organic admixtures, such as organic acids, presenting in cementitious binders are available [9,10].

In our previous work [11], it was shown that ladle slag (LS, a by-product from a steel-refining process) hydrated with gypsum to form an ettringite-based binder. Similarly to supersulfated [12] and calcium sulfoaluminate (CSA) cements [13], crystalline ettringite (AFt) is the main hydrate in the binder along with smaller quantities of monosulfate (i.e., the sulfate endmember of the AFm family [14]) and aluminum hydroxide (AH$_3$). The formation of ettringite happens rapidly, and therefore citric acid was used as a set retarder to control the workability of the binder. In addition, the acid was found to change the phase assemblage of the binder, which led to an increase in compressive

strength by up to 45% [11]. The acid has been shown to work as a retarder in the investigated ettringite-based binders to achieve the required workability and setting times, and its effects on mechanical properties are negligible [15] or even positive [11].

In the literature, the influence of organic acids and salts, particularly citric acid, is not yet clearly understood. Zajac et al. [16] investigated the effects of three commonly used retarders on CSA cement: sodium gluconate, sodium potassium tartrate, and borax. The retardation is caused by either preventing the formation of hydrates (tartrate and gluconate) or the dissolution of ye'elimite and lowering the initial pH (borax). However, the exact retardation mechanism was not identified [16]. As for the citric acid in ettringite systems, the effects of this set retarder and its mechanism of function also remain unclear. Its role in retardation has been described by several mechanisms, such as:

- complexation agent [10,17], or
- Ca-dissolution retardation in cement particles [9], and
- been assigned to its partially inhibition of gypsum formation [18].

In addition, when used at high addition levels (e.g., 2 wt%), it has been found to reduce the setting time of Portland cement, as well as to increase ettringite formation, dispersion and compressive strength [19].

This work deals with the role of citric acid as a set retarding additive in a newly developed ettringite-based cementitious binder, and how thermodynamic modelling can be used to capture its effect and to provide understanding of the hydration in the ettringite-based binders. This study aims at using thermodynamic modelling to predict the hydration of the ettringite-based binder from ladle slag and gypsum (acronym LSG) with and without the presence of citric acid. The intention is to gain insights into the hydration of LSG and its retardation by comparison with experimental data. In details, the study intends to understand:

(i) which aspects can be captured by thermodynamic modelling in the presence of citric acid as a retarder, and
(ii) what role citric acid plays in the system in addition to its function as a retarder.

A thermodynamic model was built for LSG utilizing hydration kinetics of LS as well as gypsum as input obtained from quantitative X-ray diffraction (Q-XRD). Additionally, thermodynamic data of the citric acid and citrate complexes were calculated considering existing data in the literature [9,20–23]. Therefore, the acid could be utilized in the thermodynamic model aiming to capture its effects on the binder. The influences of citric acid on the phase assemblage and microstructure were also investigated via microstructural analysis with scanning electron microscopy with energy dispersive spectroscopy (SEM/EDS). To verify the role of citric acid in a further simplified system, its morphology and mineralogy were investigated on synthesized ettringite with variation in acid dosages.

2. Materials and methods

2.1. Materials

Ladle slag (LS) was received from SSAB Europe Oy (Finland), which was naturally cooled and collected at a slag cooling pit at Raahe (Finland). The as-received slag was sieved with a 2-mm sieve to remove larger leftover steel flakes from the steel-refining process. The slag was then ground with a ball mill (filling ratio: 60%) to obtain a median particle size of approximately 10 μm, similarly to that of Portland cement. A synthetic gypsum (VWR Finland, purity $\geq$ 98%) with a median particle size of roughly 9 μm was used as the calcium sulfate source in this study without any further treatment. The chemical compositions of the LS and gypsum are shown in Table 1, analyzed by X-ray fluorescence (XRF) on a PANalytical Omnian Axiosmax (United Kingdom) at 4 kV. Fig. 1 shows the phase composition of LS and gypsum measured by Q-XRD (see Section 2.2.1) using TiO_2 (10–13 wt%) as an internal standard.

Reagent-grade citric acid (Tokyo Chemical Industry Co., Ltd., purity >98%) was used in this study as the set retarder. To synthesize ettringite, $Ca(OH)_2$ (ACS reagent, Merck, CAS: 1305-62-0) and $Al_2(SO_4)_3 \cdot 18H_2O$ (extra pure, Acros Organics, CAS: 7784-31-8) were used as precursors.

2.2. Phase characterization

The mineralogy and microstructure of LSG mixtures with different citric acid contents (0.1–2 wt% concentration) were characterized on paste samples. In this study, the focus of discussion is mainly on the plain material (i.e., LSG) and the mixture containing the highest citric acid concentration (named as LSG-Cit-2%), to capture the most distinguishable effects of citric acid, which are most clearly observable at high dosages. Therefore, only the LSG and LSG-Cit-2% mixture recipes are shown in Table 2, whereas details for other mixtures with lower citric acid content are presented in Table A1 of the Appendix.

2.2.1. XRD

Quantitative XRD analysis for paste samples was performed on powdered samples using a D2 PHASER (Bruker, Bremen, Germany) automated diffractometer, equipped with a Lynx-eye super speed position-sensitive detector. Hydration stoppage was done with solvent exchange using isopropanol. A beam knife slit was positioned 1 mm above the sample surface, and the samples were prepared using the
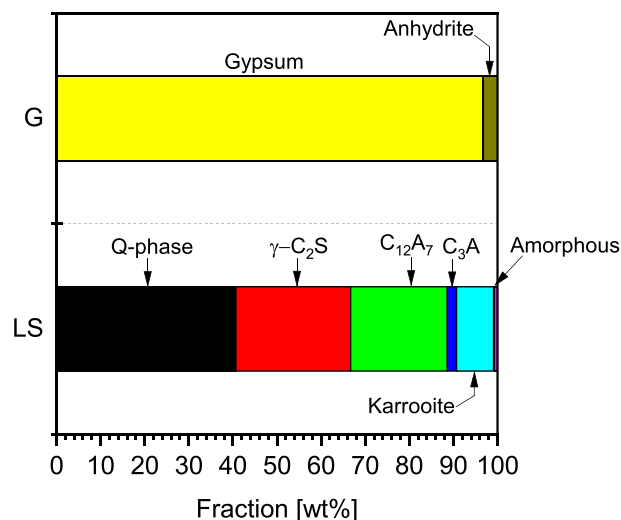

Fig. 1. The phase composition in LS and gypsum measured by Q-XRD [11].

Table 1
Chemical composition (wt%) of LS and gypsum measured by XRF.

	CaO	SiO₂	Al₂O₃	Fe₂O₃	MgO	SO₃	TiO₂	LOI at 950 °C	Others
Cement notation	C	S	A	F	M	$\bar{S}$	–	–	–
LS	50.6	13.9	24.4	0.4	3.8	0.4	4.1	1.0	1.4
Gypsum	32.3	0.7	0.1	0.1	–	42.0	–	21.3	3.1

Table 2
Mix proportions (by mass) of the LSG without and with citric acid.

Material	LS	Gypsum	W/B[a]	Citric acid[b]
LSG	0.7	0.3	0.45	–
LSG-Cit-2%				2 wt/wt% solution

[a] The W/B (water-to-binder ratio) with the total binder mass was determined by summing the mass of the slag and the gypsum.
[b] 2 wt% citric acid is dissolved in the mixing water.

back-loading technique. The detector was operated at 30 kV and 10 mA using Cu-Kα-radiation (if a different anode was used, the setup will be clarified in relevant text). The measurements were conducted in the range of 2θ = 5° to 70° 2θ, using 2θ = 0.02° 2θ step width and a counting time of 0.3 s per step. The measurements were executed in continuous position-sensitive detector fast mode, while the sample was rotated at 15 rpm. To determine the hydration kinetics of LSG, Q-XRD analyses were performed at very early stage (i.e., 1, 4, and 8 h) until 90 days of hydration. Phase assignment was done using EVA V.3.1 (Bruker AXS) software, while MAUD (i.e., Material Analysis Using Diffraction software) [24] was used based on the Rietveld method and the background was fitted by a 15 coefficient polynomial function [25,26]. As for phase quantification, ZnO (purity 99.9%, Merck) (9–11 wt%) was used as an internal standard for quantitative analysis of ground pastes.

2.2.2. SEM/EDS

The microstructure of binders at 28 days was evaluated with a Zeiss (Oberkochen, Germany) Ultra Plus field emission scanning electron microscope (FE SEM) instrument at a 15 kV accelerator voltage and a working distance of 8–10 mm. Prior to evaluation, the hydration of the samples was stopped by solvent exchange with isopropanol, and vacuum-impregnated with low-viscosity epoxy resin, polished with diamond discs of 220–1 μm at 150 rpm using ethanol as lubricant. Samples were coated carbon with a thickness of 20 nm. The pastes were observed using the backscattered-electron mode (BSE), and an Oxford EDX detector (Oxford Instrument, Oxfordshire, the UK) was used to determine the elemental distributions and composition.

To observe the morphology of synthetic ettringite with the presence of citric acid, powdered ettringite samples were coated with Pt (around 70 nm in thickness) and used secondary electron in a Zeiss Sigma (working distance: 3.3 mm and accelerator voltage: 5 kV) for observation.

2.2.3. Thermogravimetric analysis (TGA/DTG)

TGA/DTG analyses were done with a Precisa Gravimetrics AG (Dietikon, Switzerland) "prepASH" for roughly 50 mg of powdered sample. Hydration stoppage was done with isopropanol via solvent exchange prior to the analysis. Samples were transferred to alumina crucibles and heated from 23 °C to 1000 °C at a heating rate of 10 °C/min in a nitrogen atmosphere with a flow rate of 20 ml/min.

2.3. Thermodynamic modelling

Thermodynamic calculations were based on Gibbs free energy minimization using GEMS software (Paul Scherrer Institute, Villigen, Switzerland) [27,28]. GEMS is a geochemical modelling code, which can compute equilibrium phase assemblage and speciation in complex chemical systems. GEMS's default database was used and supplemented by the Cemdata18 database [5], which is a database for cementitious systems containing solubility products of the hydrated solids in the most common cementitious binders; such as AFt (including ettringite), AFm (including monosulfate) phases, hydrogarnet, and hydrotalcite [5].

Several individual phases of the raw materials were considered for the implementation of hydration kinetics, namely the Q-phase (i.e., a quaternary phase $C_{20}A_{13}M_3S_3$), mayenite ($C_{12}A_7$), gamma belite (γ-C_2S) and tricalcium aluminate (C_3A), whereas karooite and perovskite were

seen as inert, and the amorphous content in LS was considered negligible (2–3 wt% in mixtures). An empirical kinetic equation, proposed in Ref. [7], was used to implement the hydration kinetics of gypsum and the individual phases of LS. The equation utilizes input from experimentally determined degrees of hydration as a function of time for each individual phase as following [7]:

$$Q_i(t) = Q_{i0} + k_i e^{\left(-n_i/_t\right)}, \tag{1}$$

where: i indicates different anhydrous phases, which requires consideration in an equal manner; $Q_i(t)$ is the dissolved mass of anhydrous phase i at a certain time t; Q_{i0} is a constant that allows for adjustments for an initially fast dissolution/hydration of a phase; k_i is a limiting availability of a phase's mass for hydration during the period of investigation; and n_i is a parameter related to the rate of hydration for a phase. To allow for the direct calculation in GEMS, the exponent of the exponential function needs to be in the interval $-70 \leq x \leq 70$, which may restrict the hydration times investigated. If necessary, the function can be solved in another software and be implemented as a column of hydration factors ($0 \leq f(x) \leq 1$) into GEMS.

The thermodynamic data including log K_{S0} and ΔS^0 of citric acid were added into GEMS's database according to their available properties reported in Ref. [9, 20] considering the complexation between citrates and different species (Table 3).

To facilitate the description of the acid in the database, a citrate ligand, named *Cit*, was created as an independent component with the thermodynamic properties shown in Table 4. In addition, a citrate ion (Cit^{3-}) was created as a dependent component in the database using the thermodynamic data of the citrate ligand *Cit*.

2.4. Ettringite synthesis

The CaO/Al_2O_3 molar ratio was fixed at 6:1 for all ettringite synthesis similarly to Goetz-Neunhoeffer et al.'s work [29]. The crystals

Table 3
Thermodynamic data for citrate and its complexes referring from Ref. [9, 20–23] with citric acid = H_3Cit.

Species	Reaction	log K_{S0}	ΔS^0
Aqueous			
$HCit^{2-}$	$HCit^{2-} \leftrightarrow Cit^{3-} + H^+$	−6.36	
H_2Cit^{1-}	$H_2Cit^- \leftrightarrow HCit^{2-} + H^+$	−4.78	−83.46
H_3Cit^0	$H_3Cit^0 \leftrightarrow H_2Cit^- + H^+$	−3.13	−44.83
CaH_2Cit^+	$CaH_2Cit^+ \leftrightarrow H_2Cit^- + Ca^{2+}$	1.53	–
$CaCit^-$	$CaCit^- \leftrightarrow Cit^{3-} + Ca^{2+}$	4.8	91.89
$CaHCit$	$CaHCit \leftrightarrow HCit^{2-} + Ca^{2+}$	2.92	–
$AlCit$	$AlCit + H^+ \leftrightarrow AlHCit^+$	−2.5	–
$AlCitOH^-$	$AlCit \leftrightarrow AlCitOH^- + H^+$	−3.4	–
$AlHCit^+$	$AlHCit^+ \leftrightarrow Al^{3+} + HCit^{2-}$	−32.87	–
$Fe(Cit)_2^{3-}$	$2Cit^{3-} + Fe^{3+} \leftrightarrow Fe(Cit)_2^{3-}$	11.64	–
$Fe(Cit)_2H^{2-}$	$2Cit^{3-} + Fe^{3+} + H^+ \leftrightarrow Fe(Cit)_2H^{2-}$	14.84	–
$Fe(Cit)_2OH^{4-}$	$2Cit^{3-} + Fe^{3+} + H_2O \leftrightarrow Fe(Cit)_2OH^{4-} + H^+$	7.51	–
$FeCit$	$Fe^{3+} + Cit^{3-} \leftrightarrow FeCit$	7.67	–
$FeCitOH^-$	$Cit^{3-} + Fe^{3+} + H_2O \leftrightarrow FeCitOH^- + H^+$	5.48	–
K_2Cit^-	$2K^+ + Cit^{3-} \leftrightarrow K_2Cit^-$	1.39	–
$KCit^{2-}$	$K^+ + Cit^{3-} \leftrightarrow KCit^{2-}$	1.03	–
$MgCit^-$	$Mg^{2+} + Cit^{3-} \leftrightarrow MgCit^-$	4.81	–
$MgHCit$	$Mg^{2+} + HCit^{2-} \leftrightarrow MgHCit$	2.6	–
MgH_2Cit^+	$Mg^{2+} + H_2Cit^- \leftrightarrow MgH_2Cit^+$	1.31	–
Na_2Cit^-	$2Na^+ + Cit^{3-} \leftrightarrow Na_2Cit^-$	1.81	–
$NaCit^{2-}$	$Na^+ + Cit^{3-} \leftrightarrow NaCit^{2-}$	1	–
Solids			
$Ca_3Cit_2(H_2O)_4$	$2Cit^{3-} + 3Ca^{2+} + 4H_2O \leftrightarrow Ca_3Cit_2(H_2O)_4$	17.9	–
$K_3Cit.H_2O$	$K_3Cit.H_2O \leftrightarrow Cit^{3-} + 3K^+ + H_2O$	−1.24	–
KH_2Cit	$KH_2Cit \leftrightarrow H_2Cit^- + K^+$	−6.21	–
Na_2H_2Cit	$Na_2H_2Cit \leftrightarrow H_2Cit^- + Na^+$	−4.87	–
$Na2HCit$	$Na2HCit \leftrightarrow HCit^{2-} + 2Na^+$	−3.94	–
$Na_3Cit.H_2O$	$Na_3Cit.H_2O \leftrightarrow Cit^{3-} + 3Na^+ + 2H_2O$	−1.19	–
H_3Cit	$H_3Cit.H_2O \leftrightarrow H_3Cit + H_2O$	−1.33	–

Table 4
Data for citrate ligand (*Cit*) calculated as independent component in GEMS.

Ligand	Atomic mass (M_{0i})	Standard-state absolute entropy (S_{0i})	Formula charge (*Valens*)	Standard-state absolute heat capacity (Cp_{0i})	Standard state volume (V_{0i})
Cit	189.1	218.91	−3	−75.36	−1.8

were formed from dissolved $Ca(OH)_2$ (concentration $c_{CaO} = 68$ mmol/l) and a solution of $Al_2(SO_4)_3 \cdot 18H_2O$ (concentration $c_{Al2(SO4)3} = 11.4$ mmol/l). The acid's concentration varied from 0.45 to 1.8 mmol/l, whereas the plain sample was synthesized without the presence of citric acid. Different synthetic ettringite mixtures were synthesized at room temperature (approximately 23 °C) for 2 days in sealed conditions to prevent carbonation. The precipitated ettringite was filtered via vacuum filtration and washed with isopropanol for 2 times for hydration stoppage and removal of leftover precursors (if any), dried in an oven at temperatures below 40 °C for 1 h, and kept in a desiccator prior to its characterization with XRD, TGA, and SEM.

3. Results

3.1. Hydration kinetics

Citric acid had varying influence on the hydration kinetics of the main anhydrous phases. Table 5 shows a comparison of the degrees of hydration of the different anhydrous phases in LSG without and with 2 wt% citric acid, while Fig. 2 shows the DTG of these pastes at different hydration times. The citric acid reduced the rate of hydration of Al-containing phases in the binder. $C_{12}A_7$ reacted quickly with quarter of the phase hydrated after a half day. This explains the formation of ettringite in minutes after the hydration between LS and gypsum observed via in-situ XRD [11]. The entire amount of gypsum was consumed after 7 days of hydration. On the other hand, Q-phase had lower degree of hydration at 1 day, but similar quantities of this phase were dissolved after 90 days. Gamma-C_2S exhibited low hydration kinetics due to the low reactivity of this olivine mineral [30].

With the presence of 2 wt% citric acid solution, the hydration degree of Al-containing phases in LS dropped by roughly 20–30% compared to the plain LSG paste at 1 day. However, at later hydration stages (i.e., after 14 days of hydration), the degree of hydration of these phases was identical for both mixtures regardless the presence of citric acid. This is similar to the phase evolution of CSA cement in the presence of citric acid, reported in Ref [31]. The fraction of C_3A in the mix compositions is relatively low (ca. 2 wt%), and hence Q-XRD result might not determine precisely the degree of hydration of this phase. Interestingly, citric acid significantly increased the reaction degree of γ-C_2S throughout the tested period.

Ettringite formed rapidly in the first hours of hydration, while citric acid delayed its precipitation and most of the gypsum remained unreacted after 1 day (Fig. 2). However, the thermogravimetric behaviors of LSG with and without citric were identical after 28 days of

hydration, except for a slight mass loss at 950 °C in LSG-Cit-2% sample. This is possibly due to the reduction–oxidation reaction of SO_4^{2-} in the presence of citric acid and potentially the effects of citric acid on changing the crystal structure of ettringite; some evidences are reported in Section 3.3.

3.2. Microstructural analysis

The microstructural analysis by SEM/EDS shows indistinguishable phase assemblages between LSG and LSG-Cit-2% including AFt, AFm, AH_3, C–(A–)S–H, and remaining reactants. The microstructures, represented by SEM images in Fig. 3, shows a higher degree of hydration in LSG-Cit-2% than that of plain LSG. This is related to a higher reaction degree of γ-C_2S (see Table 5), as the other reactants have similar degree of hydration at that time. In addition, the EDS results confirm AFt and AFm as the main hydration products (Fig. 4b), while AH_3 and C–(A–)S–H gel are present as minor phases together with some unreacted LS (Fig. 4a). As common for cementitious binders, the level of intermixing is high for these phases due to the relation between interaction volume and crystallite sizes and explains the scatter around the theoretical ratios (Fig. 4b). With the presence of citric acid in LSG, the compositions shift toward more AFt formation and less AFm in comparison to the plain paste. Fig. 4b also shows an intermixing/composition of AFt, AH_3, AFm (mostly monosulfate), while carbonated phases such as mono and/or hemicarbonate and calcite were not found via XRD analyses. The C–(A–)S–H gel formed together with amorphous aluminum hydroxide is likely due to the deficiency of Ca in the system. Notably, the gel is not thermodynamically predicted to be stable in the binder and should eventually convert to a more stable phase (i.e., strätlingite) as reported by Jeong et al. [32] and the thermodynamic calculation discussed in Section 4.1.

Moreover, the W/B ratio plays an important role in affecting the phase assemblage of the binder. Fig. A1 (see Appendix) also shows evidence for the formation of strätlingite in LSG with a change in W/B ratio. A higher W/B ratio can lead to a higher degree of hydration by facilitating the dissolution of γ-C_2S as well as Al-containing phases and a more porous microstructure (see Fig. A2 in the Appendix). This explains the precipitation of strätlingite for this binder with higher W/B ratios where silicon dissolved from γ-C_2S and the Q-phase. Furthermore, magnesium aluminate spinel ($MgO.Al_2O_3$) was found only in LSG paste with W/B = 1 (ca. 5 wt% via Q-XRD analysis). Backscattered SEM images, such as Fig. A2a, show the presence of spinel with Mg/Al atomic ratio around 0.7 (Fig. A3), whereas spinel was not found in LSG pastes with lower W/B ratio.

3.3. Synthetic ettringite in the presence of citric acid

Figs. 5–7 show the mineralogy (XRD and DTG analyses) and morphology (SEM using a secondary electron detector) of synthetic ettringite, respectively, with and without the presence of citric acid. Gypsum and monosulfate were found to precipitate together with ettringite in the presence of 1.8 mmol/l citric acid. No difference in
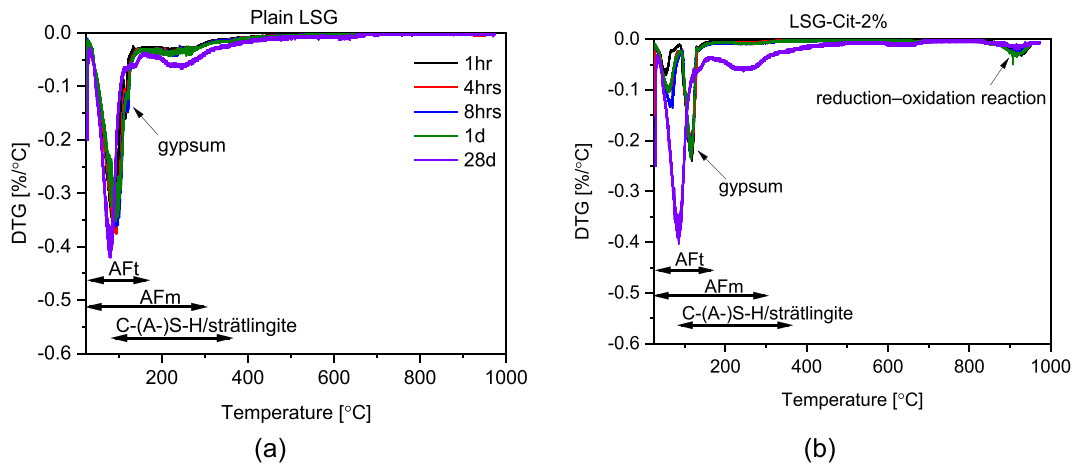
Table 5
Degrees of hydration (%) for individual phases in paste samples of LSG and LSG-Cit-2% from Q-XRD results (estimated error 5%).

Time (days)		0.5	1	3	7	14	28	60	90
LSG	$C_{12}A_7$	25.9	41.8	88.9	91.7	88.1	89.7	98.1	100
	Q-phase	14.4	39.8	49.7	78.4	80.8	82.4	83.5	87.4
	C_3A	63.0	68.4	97.9	99.4	100	100	100	100
	γ-C_2S	0	2.1	5.3	11.3	14.3	15.1	17.4	26.2
	Gypsum	78.1	79.4	88.7	99.3	96.0	98.1	100	100
LSG-Cit-2%	$C_{12}A_7$	12.7	17.9	44.8	58.9	96.3	91.5	94.4	100
	Q-phase	0	0	55.9	44.4	52.0	83.8	85.0	87.1
	C_3A	0	100	100	100	100	100	100	100
	γ-C_2S	0	7.0	15.5	35.1	27.7	34.5	38.5	34.0
	Gypsum	21.1	24.2	64.2	69.0	96.1	98.3	98.7	98.7

Fig. 2. DTG analyses of (a) plain LSG and (b) LSG-Cit-2% from 1 h to 28 days of hydration.
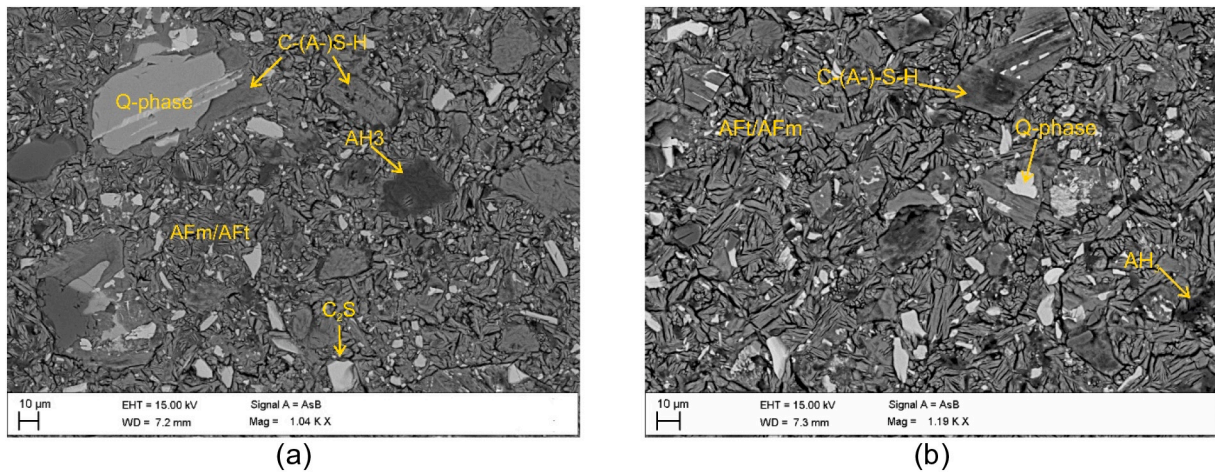

Fig. 3. Microstructure of (a) plain LSG, (b) LSG-Cit-2% after 28 days of hydration.
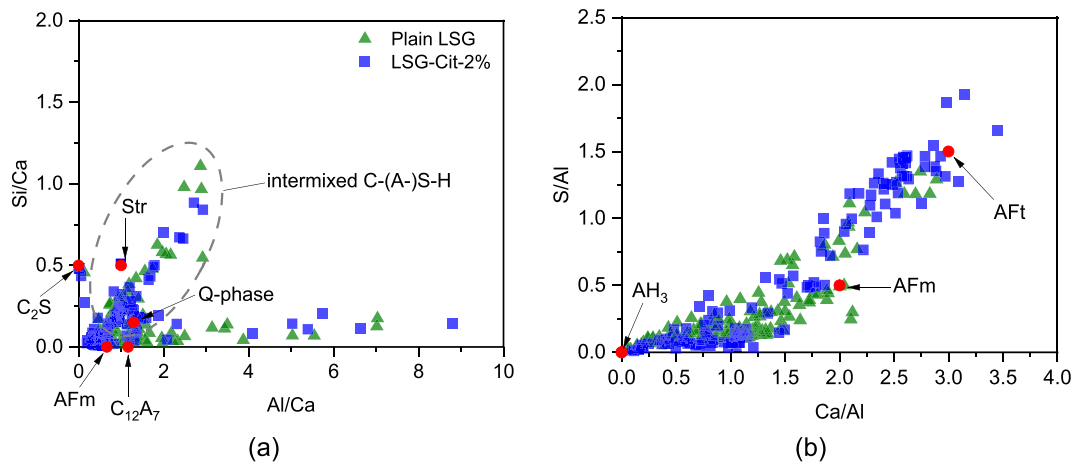

Fig. 4. Atomic ratio plots obtained from EDS analysis for LSG (green dots) and LSG-Cit-2% (blue dots) after 28 days whereas the theoretical atomic ratios of specific reactants and hydrate phases (Str: strätlingite, AFt: ettringite, and AFm: monosulfate) are indicated by red dots. (For interpretation of the references to color in this figure legend, the reader is referred to the web version of this article.)

morphology and precipitation of synthesized ettringite was observed compared to the crystals synthesized without citric acid for lower citric acid concentrations (0.45 and 0.9 mmol/l). The ettringite morphology displayed long thin needle-shaped crystals as shown in Fig. 7a. In contrast, with 1.8 mmol/l citric acid used in the synthesizing solution, the acid altered the morphology of the ettringite crystals as the binder formed small quantities of gypsum and monosulfate along with the ettringite. Gypsum was detected by XRD and EDS analysis with
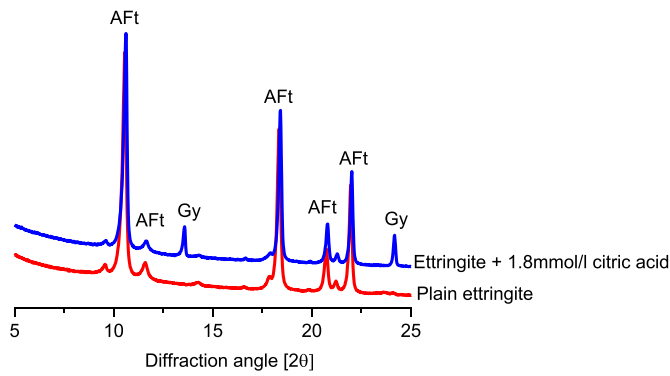
Fig. 5. XRD diffractograms of synthetic ettringite with and without citric acid; note the precipitation of gypsum (Gy) in the presence of 1.8 mmol/l citric acid.
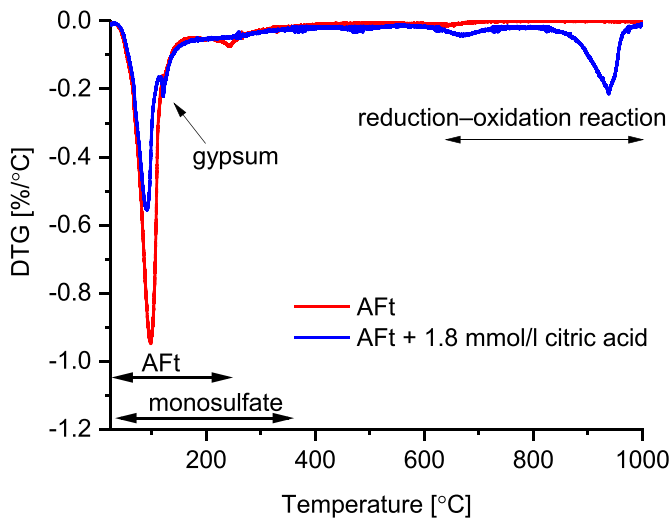

Fig. 6. DTG of synthesized ettringite with and without the presence of citric acid; note that no carbonated phases were found in both XRD and TGA.

reflections at approximately 13 and 24° 2θ. The quantification of monosulfate via XRD patterns is difficult, due to its low crystallinity and overlapping reflections with ettringite. The slight mass loss in the TGA/DTG experiments at around 200–350 °C was assigned to this precipitate (Fig. 6 for synthetic ettringite with 1.8 mmol/l citric acid). Gypsum and

monosulfate were observed in proximity to ettringite in the secondary-electron SEM micrograph shown in Fig. 7b.

Notably, there was a mass loss in a range of 600–1000 °C observed on the synthetic ettringite with the presence of citric acid (Fig. 6). This mass loss can possibly be attributed to the reduction–oxidation reaction of SO_4^{2-} in the presence of organic carbon of citric acid, which was similarly observed by Goetz-Neunhoeffer et al. [29] in synthetic ettringite with the presence of sucrose. It is possible that the crystal structure of ettringite was altered in the presence of citric acid. Hence, this behavior deserves a more thorough investigation on the crystallography of ettringite under the effects of organic ligands, which is suggested as a future study, but out of the scope of the here presented work.

With a fixed CaO/Al_2O_3 molar ratio of 6:1 in the system, ettringite precipitated as indicated in the reaction described in Eq. (2). However, citric acid promoted another reaction path to form monosulfate and gypsum as shown in Eq. (3) together with the formation of ettringite. In the presence of 1.8 mmol citric acid, monosulfate and gypsum formed 21.8 and 5.2 wt% of the binder, respectively, and ettringite constituting around 73.0 wt% via Q-XRD analysis.

$$6CH + A\overline{S}_3 + 26H \rightarrow C_3A \cdot 3C\overline{S} \cdot 32H \qquad (2)$$

$$6CH + A\overline{S}_3 + 10H \rightarrow C_3A \cdot C\overline{S} \cdot 12H + 2C\overline{S} \cdot 2H \qquad (3)$$

4. Discussion

4.1. Modelling and experimental results

The Q-XRD data (shown in Table 5) were used as the kinetic input of the thermodynamic model. This approach was chosen to account for the reaction kinetics, as the results of the modelling without kinetic input resulted in differences of up to ca. 25% in the amount of precipitates compared to the experimental data reported in Section 3.1. Table 6 shows the input parameters used in Eq. (1) to represent the hydration kinetics of the LS's phases and gypsum as in Ref. [7].

The curves in Fig. 8 represent the calculated dissolved quantities of each individual phase compared to the experimental result shown as symbols in Table 5. The Al-containing phases, namely i.e. Q-phase and $C_{12}A_7$, exhibited very fast dissolution ($n = 0.45$ and 0.25, respectively) and high degree of hydration with k values of 85 and 93, respectively. The $C_{12}A_7$ is known as a highly reactive phase, which can accelerate the hydration in ettringite-based binders [11,33]. The Q-phase also shows a high hydraulic activity as the main crystalline anhydrous phase in LS (Fig. 1). In contrast, γ-C_2S is poorly reactive [34] with a slow dissolution rate ($n = 3$) and hence a low hydration degree ($k = 23$) in the period of
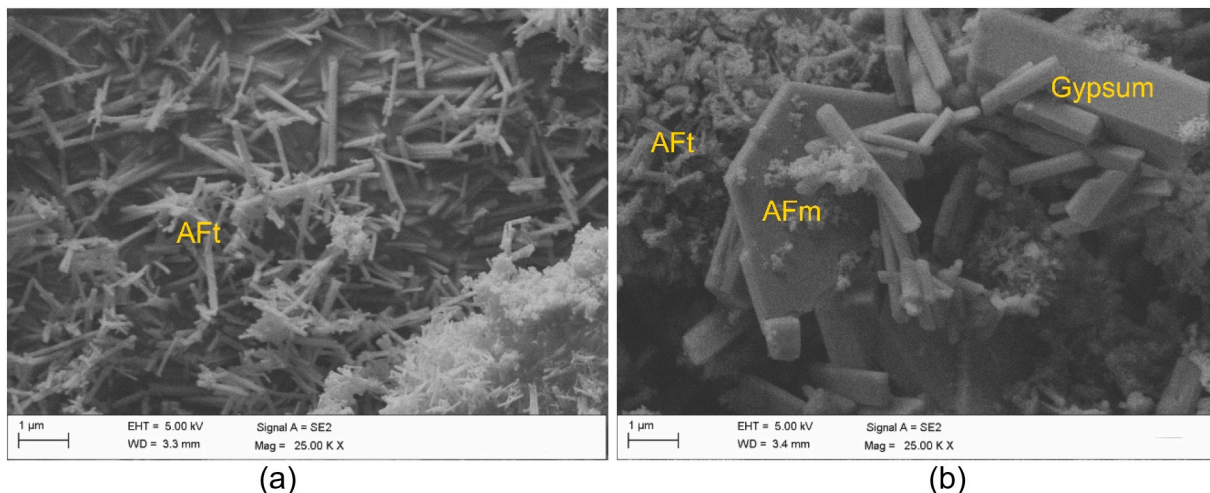

Fig. 7. Morphology of synthesized ettringite (a) without and (b) with the presence of citric acid.

Table 6
Parameters used in Eq. (1) for modelling the hydration kinetics of phases in LS and gypsum.

Phase	Q_0	N	k
Q-phase	0	0.45	85
$C_{12}A_7$		0.25	93
γ-C_2S		3.00	23
Gypsum		0.14	100

observation. As for gypsum, the phase often dissolves completely at the beginning of hydration [13]. In this work, the dissolution of gypsum was also fast as the system had dissolved all available gypsum after ca. 10 days of hydration.

From the proposed kinetics model, the calculated phase assemblage for LSG binders without citric acid and in its presence were identical as shown in Fig. 9. Ettringite forms rapidly at a very early age of hydration, which is confirmed by in-situ XRD diffractograms after 13 min of hydration [11]. Monosulfate appeared also at early hydration stages (less than 1 day) and occupied the highest fraction in the binder at later stage, in which the phase showed very poor crystallinity, and hence was often underestimated in both in- and ex-situ XRD analyses [11,35]. Amorphous AH$_3$ was experimentally found in this study but not gibbsite (i.e., crystalline AH$_3$). Hence, the latter was switched off in the thermodynamic model. In other ettringite-based system (i.e., belite–ye'elimite–ferrite [36]), amorphous CAH$_{10}$ and AH$_3$ may precipitate at early hydration; in contrast, calcium aluminate hydrates were not thermodynamically predicted to form in LSG, also not observed experimentally. Once strätlingite started to precipitate the fraction of ettringite reduced, which was similarly reported in Ref. [36].

Hence, solid-state ^{27}Al MAS NMR was used as analytical technique to quantify the monosulfate to ettringite ratio in these binders, as this technique also detects also aluminum coordinations, which can be X-ray amorphous. The presence of monosulfate in LSG binders combined with a reduced ettringite formation indicates the undersulfation of the binder or the depletion of available water for further hydration reactions. AH$_3$ gel was determined by solid-state ^{27}Al MAS NMR with a chemical shift of 5.0 ppm in the LSG paste [11]. This is a secondary hydrate from the reaction between Al-containing phases and calcium sulfate sources along with primary phase of either ettringite or monosulfate [13,37,38]. The modelling suggests the precipitation of strätlingite as a Si-bearing phase that may precipitate when the γ-C_2S and/or Q-phase ($C_{20}A_{13}M_3S_3$) hydrate. Furthermore, OH-hydrotalcite (i.e., Mg–Al layered double hydroxide) was formed as a minor precipitate due to the dissolution of Q-phase providing a small fraction of magnesium in the hydrated cement. The hydrotalcite was found surrounding Q-phase grain due to the low mobility of Mg at high pH [39] with a Mg/Al atomic ratio of ca. 2 (Fig. A4).

The thermodynamic model, which considered the hydration kinetics of LS and gypsum, can predict precisely the delay in ettringite formation with different dosages of citric acid. Note that the model can capture this effect of citric acid on LSG only when the kinetics of precursors are implemented. Fig. 10 shows the good agreement between in-situ XRD (reported in Ref. [11]) and thermodynamic calculations for the onset of ettringite formation. This revealed the rapid formation of ettringite in the binder without the presence of citric acid, whereas the precipitation is delayed by almost 2 h with 2 wt% citric acid solution in the system. Based on the thermodynamic model, citric acid reduces the pH in the pore solution of the binder from ca. 12 to below 9.5 during the first hours
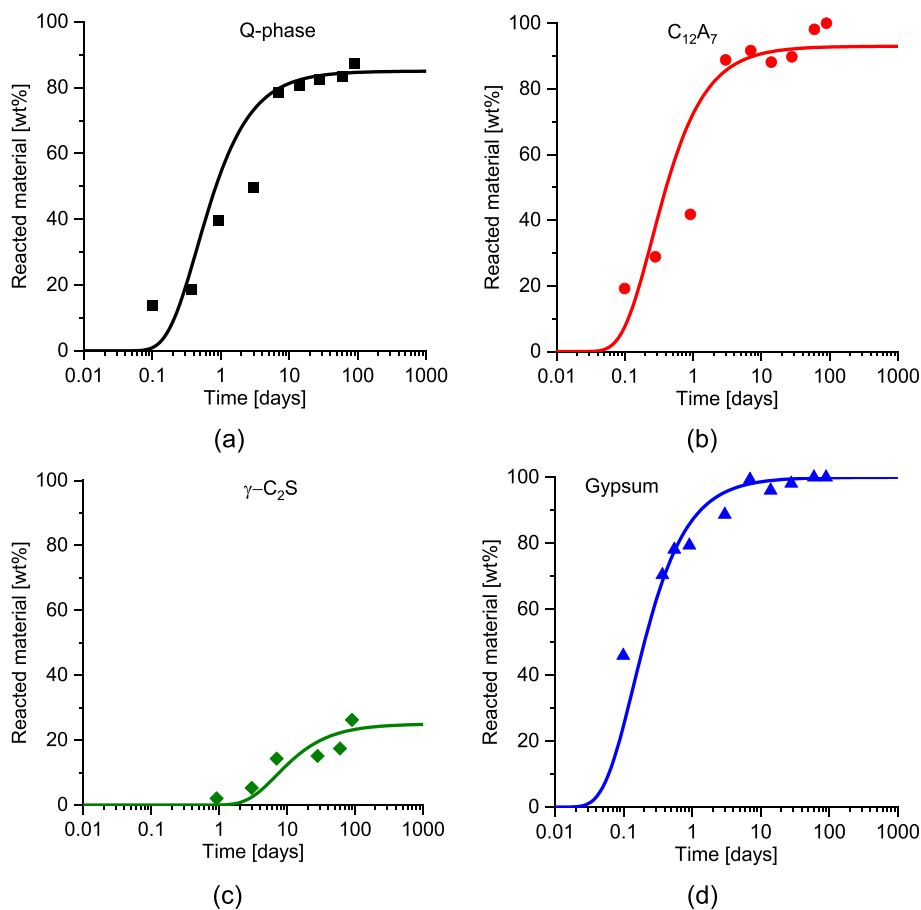

Fig. 8. The experimental data (symbols) and modelling (continuous lines) of the degree of hydration of (a) Q-phase, (b) $C_{12}A_7$, (c) γ-C_2S in LS, and (d) gypsum from the beginning to 90 days of hydration. C_3A followed the hydration kinetics model based on Parrot and Killoh [6,8].
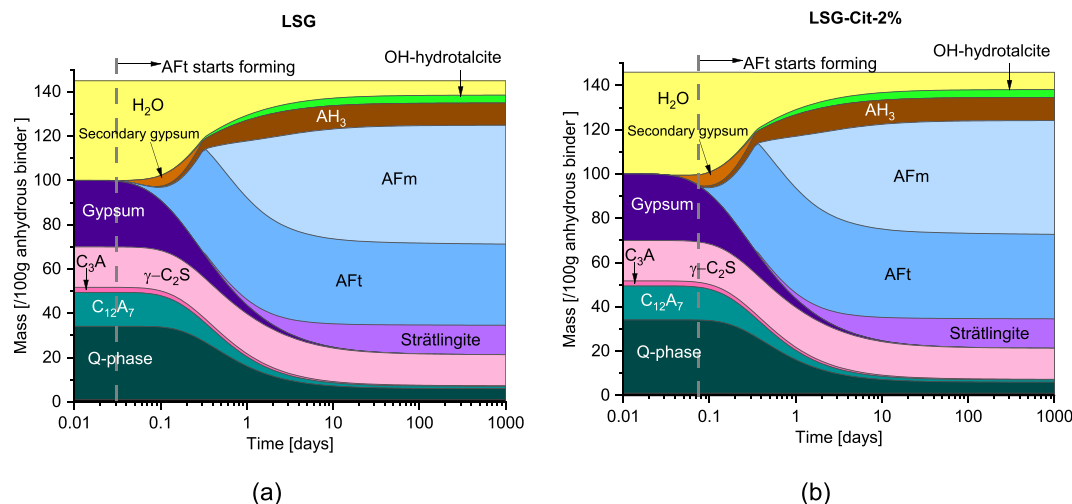
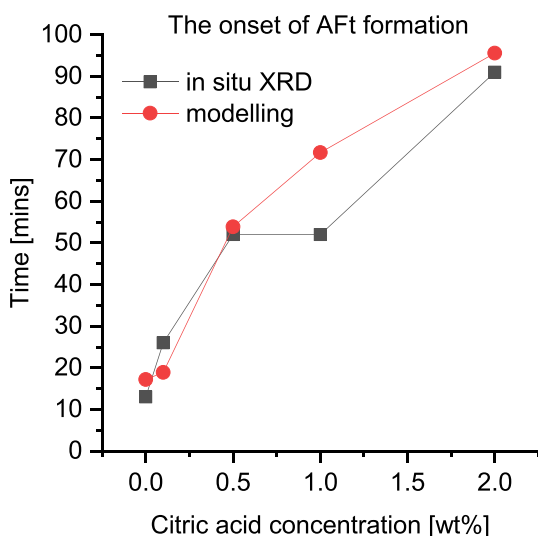**Fig. 9.** The modelled phase assemblage of (a) plain LSG and (b) LSG-Cit-2%.

Fig. 10. The comparison between in-situ XRD (referred data from Ref. [11]) and thermodynamic modelling for the onset of AFt formation with different citric acid content.

of hydration. Therefore, the precipitation of crystalline ettringite could be related to changes in the pH. In contrast, in the absence of citric acid, ettringite was always oversaturated and stable in the hydrated binder.

Fig. 11 shows the comparison of the predicted hydrates quantities (i. e. AFt and amorphous content) based on thermodynamic modelling for LSG without and with citric acid compared to experimental results from Q-XRD. In the case of plain LSG, the thermodynamic model predicts the ettringite quantities well throughout the whole hydration process (Fig. 11a and c).

In the case of 2 wt% citric acid concentration, the model over-estimates the ettringite quantities observed experimentally (Fig. 11b and d). The reason is likely to be a fundamental feature of the thermo-dynamic calculations, which calculate the thermodynamic equilibrium in the phase assemblage. Apparently, the thermodynamic data used for ettringite in combination with citric acid and its complexes in this study is not able to accurately model quantities of ettringite formed while providing good results in the absence of the acid. The retardation of hydrate formation caused by citric acid in this ettringite-based binder could possibly be modelled by adjusting the solubility of these com-pounds. However, such an approach is problematic as one undermines

the concept of thermodynamic by adjusting the solubility after demand, especially for otherwise successfully used and well-established data sets. The combination of experimental data and modelling results may be resolved if one interprets the function of citrate acid in this binder as a kinetic barrier, for example by preventing nucleation and crystal growth of ettringite and thus changing the solubility of the mineral, which fa-cilitates the formation of monosulfate (Section 3.3). More details about the effects of citric acid on the phase assemblage and particularly on the ettringite is provided in Section 4.2. At later stages of hydration, how-ever, there was a good agreement between the model and experimental results of LSG-Cit-2% after 14 days onward (Fig. 11b). Regarding amorphous and/or low-crystallinity phases in the binder (i.e., AFm and AH_3), the prediction of the thermodynamic model was in-line with the Q-XRD results.

Strätlingite was not found in LSG by XRD regardless the citric acid content, but the phase was suggested in the model since GEMS calcu-lated the equilibrium state of the phase assemblage in the hydrated binder. Therefore, ^{29}Si MAS NMR should be done in a future investi-gation to check whether strätlingite is present in the binder or not. It has been reported that C–(A–)S–H phase converts to strätlingite, which is the thermodynamically favorable hydrate in the system [5,32], if sufficient water is present. Fig. A1 shows XRD diffractograms that confirmed the precipitation of strätlingite in the LSG binder with a W/B ratio of 1. This mix also exhibited a higher hydration degree compared to that of W/B = 0.45 via SEM images in Fig. A2.

For the sake of understanding the difference between experimental results and modelling of ettringite precipitation at early stage (Fig. 11d), a thermodynamic model of LSG-Cit-2%, based on the input from Q-XRD for the hydration kinetics of individual phases of LS and gypsum, was built and compared with the experimental results and the prediction in Fig. 9b. Table 7 shows parameters of phases present in LS and gypsum that were used in Eq. (1) to represent their hydration kinetics (shown in Table 5). It can be seen that the rate of hydration of all phases was significantly lower (i.e., inversely proportional to *n* value) than that of plain LSG due to the retardation effects of citric acid. Möschner et al. [9] suggested that citrate might form a protective layer around Portland cement clinker grains and thus, retarded the dissolution of the clinker phases. This can be also one of the retardation mechanisms of citric acid in reducing the dissolution rate of phases in LS. Note that gypsum was assumed to be readily available in the mix ($Q_0 = 14$) since the phase can quickly dissolve regardless of the presence of citric acid.

Fig. 12 shows the modelling for phase assemblage of LSG-Cit-2% and a good prediction for the precipitation of hydrates in the paste. Ettringite was predicted to form after 1.5 h of hydration in which the phase occupied around 10 wt% of the paste. Due to the lack of calcium and
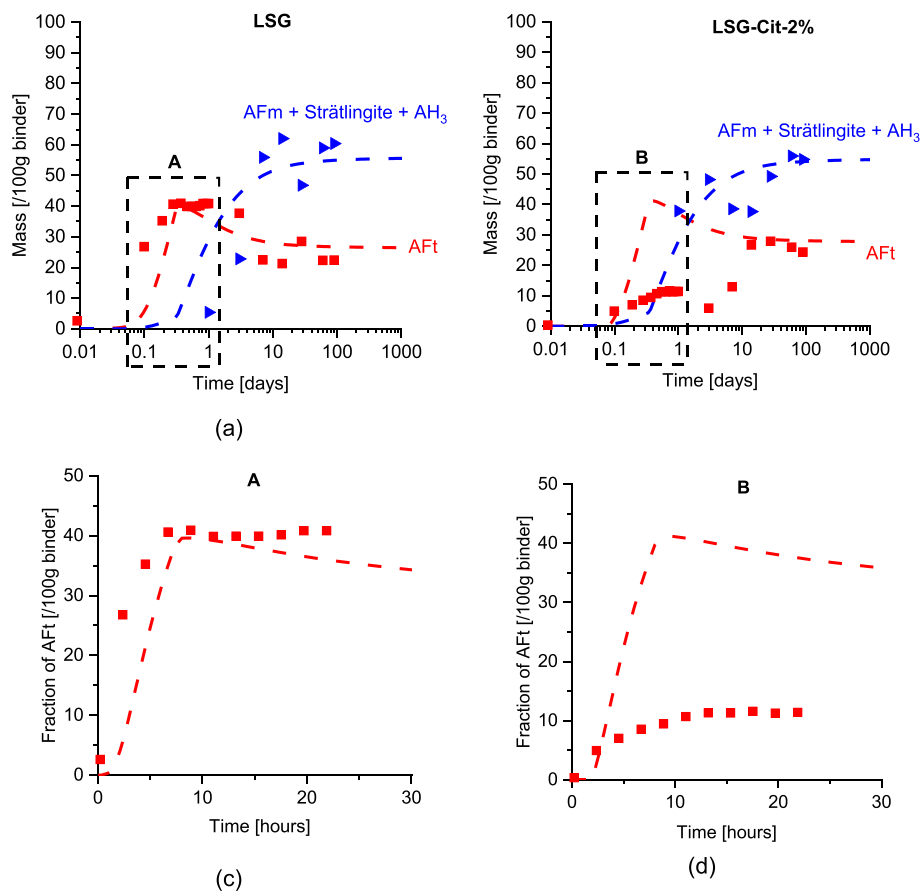
Fig. 11. The quantification of hydrates in (a, c) plain LSG and (b, d) LSG-Cit-2% in comparison between experimental results from XRD (dots) and thermodynamic modelling (lines).

Table 7
Parameters used in Eq. (1) for modelling the hydration kinetics of phases in LS-Cit-2% paste.

Phase	Q_0	n	k
Q-phase	0	2	85
$C_{12}A_7$		1.7	95
γ-C_2S		2	35
Gypsum	14	3.1	84

aluminum in the system, ettringite dissolved between 1 and 3 days of hydration to precipitate monosulfate, which is thermodynamically more stable than ettringite under the given circumstances [5]. Once there are again sufficient calcium and aluminum ions provided from the dissolution of precursors, ettringite formation continued from 3 days and reached a stable phase assemblage after 28 days. The predicted ettringite evolution in LSG-Cit-2% is in very good agreement with the experimental results (Fig. 12b). In contrast, the model in Fig. 9b overestimated the formation of ettringite at early stage (Fig. 11b) since the purely thermodynamic consideration did not capture changes in hydration kinetics of phases in LS under the effects of citric acid as discussed previously.

Citric acid increased the degree of hydration of γ-C_2S leading to a larger quantity of strätlingite predicted to precipitate. With 2 wt% citric acid solution, γ-C_2S increased its hydration degree by approximately 10% (Table 5). A hypothesis can be the complexation between citrate and calcium in γ-C_2S leading to an increase in the dissolution of this phase. In addition, γ-C_2S has olivine structure, and organic ligands are known to enhance the dissolution rate of this structure as reported in Ref. [40]. Hence, the amount of strätlingite in the binder rose by roughly

65% to account for 19% of total hydrates' mass. In contrast, the model suggests lower precipitation of AH₃ gel in order to provide aluminum for strätlingite's formation (Fig. 9b vs. Fig. 12a). There was negligible difference in the fraction of ettringite and monosulfate in LSG-Cit-2% between the two models.

4.2. The effects of citric acid on the phase assemblage of LSG

Based on the experiment on synthetic ettringite, it can be noticed that citric acid affects the precipitation of ettringite leading to the formation of some minor hydrate phases which otherwise are not stable. With the sufficient concentration of citric acid in ettringite suspension, monosulfate and gypsum can form as minor hydrates (Section 3.3). The organic ligand can also possibly change the crystal structure of ettringite; this effect will need a further study on the crystallographic analysis for ettringite precipitated with the presence of citric acid. The complexation of citrate with Ca and Al has been discussed by other researchers [10,41], however this seems not the case for the influence of citric acid on ettringite since there were no differences in the precipitation of ettringite with the concentration of citric acid lower than 1.8 mmol/l, however no measurements of total concentrations in the pore solution were conducted. Another explanation for the change in precipitates is the partial inhibition of ettringite nucleation and growth caused by citric acid, in which the negative charge of citrate compensated the positive surface charge of ettringite [42]. This may prevent the precipitation of ettringite once there is enough citrate available in solution. Hence, this could stabilize the formation of monosulfate and gypsum instead. Cody et al. [42] also observed the precipitation of monosulfate as a minor hydrate in synthetic ettringite with the presence of various chemicals and admixtures. These findings, together with our
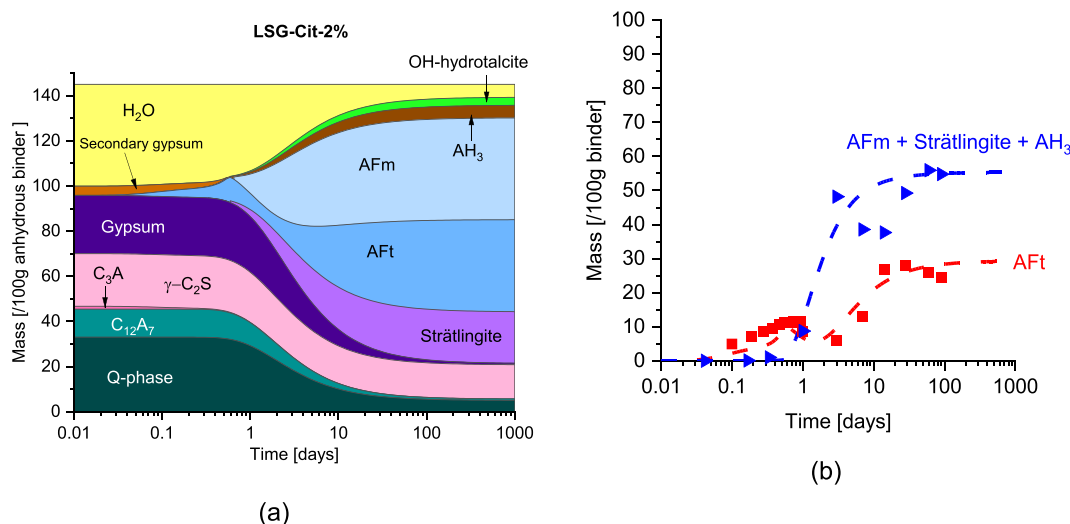
Fig. 12. (a) The modelled phase assemblage based on Q-XRD results for LSG-Cit-2% and (b) the quantification of hydrates in comparison between experimental results from Q-XRD (dots) and thermodynamic modelling (dashed lines).

own data, strengthen the argument that citric acid might work as an inhibitor of ettringite nucleation. In addition, the investigation in the synthetic ettringite done in this work can explain the increase in the fraction of monosulfate in LSG with the presence of citric acid as reported in our previous work [11].

Furthermore, citric acid alters the hydration kinetics and reaction degree of Al-containing phases and γ-C$_2$S. While the acid reduces the dissolution rate of C$_{12}$A$_7$ and Q-phase in LS at early age, it does not change the reaction degree at later stage. This leads to a delay in ettringite formation at early stage of hydration and hence prolong the setting time causing citric acid to function properly as a set retarder for ettringite-based binders. In contrast, citric acid promotes a higher hydration degree of γ-C$_2$S leading to a higher precipitation of C–(A–)S–H gel (or strätlingite based on thermodynamic calculation) since there is more silicon and calcium available in the system. Notably, the W/B ratio also plays an important role increasing the hydration degree of LSG as discussed in Section 4 and the Appendix. Once there is a higher amount of hydrates in LSG with citric acid, the compressive strength increased by up to 45% in LSG-Cit-2% compared to the plain LSG at 28 days of hydration as characterized previously in Ref. [11]. Work of other researchers reported [15,43], on the other hand, negligible or slight reduction in the compressive strength of CSA cement mortars using citric acid as a retarder. The absence of γ-C$_2$S in CSA cement can be attributed to the negligible change in compressive strength of this cement compared to LSG. Therefore, selection of an appropriate set retarder for ettringite-based binders can bring a twofold benefit without compensating or even with increasing the mechanical properties.

5. Conclusions

The present study provides insights into the retardation mechanism of citric acid in an ettringite-based binder. Thermodynamic modelling using GEMS was used to shed light on the hydration of the binder with the presence of citric acid considering the hydration kinetics of precursors (i.e., LS and gypsum) and citrate complexations. Findings in this study help to improve our understanding of the role of organic admixtures (specifically citric acid) in ettringite-based binders such as supersulfated and CSA cement, and hence offer better utilization the admixtures in these binders.

The ettringite-based binder hydrates rapidly forming ettringite in minutes after the exposure of LS and gypsum to water due to the fast dissolution of Al-containing phases in LS (i.e., mainly Q-phase and C$_{12}$A$_7$). Citric acid seems to delay the precipitation of ettringite likely

through the inhibition of ettringite nucleation and crystal growth that facilitates the formation of monosulfate and gypsum. Complexation of citrate ligand is thermodynamically weak and thus is not likely the driving factor behind the retardation by citric acid. Citric acid enhances the dissolution of γ-C$_2$S (an olivine crystal) leading to higher precipitation of C–(A–)S–H gel (or strätlingite based on thermodynamic calculation), while it reduces the dissolution of C$_{12}$A$_7$ and Q-phase at early age.

Thermodynamic modelling can predict precisely the phase assemblage of LSG and the onset of ettringite's precipitation with the presence of citric acid when dissolution rates are adjusted to match the observed rates. Ettringite, monosulfate, aluminum hydroxide, and strätlingite are suggested as main hydrates in the binder. Note that C–(A–)S–H gel was experimentally found instead of strätlingite because of the lack of water in the system. However, the thermodynamic model overestimates the fraction of ettringite at early hydration stage in LSG with 2 wt% citric acid solution. According to the hypothesis put forth, this is due to citrate blocking the nucleation of ettringite, and thus GEMS cannot capture this kinetic barrier from the ligand.

CRediT authorship contribution statement

- Hoang Nguyen: Conceptualization, Data curation, Formal analysis, Investigation, Methodology, Visualization, Writing - Original Draft, Review & Editing
- Wolfgang Kunther: Conceptualization, Methodology, Data curation, Formal analysis, Investigation, Writing - Review & Editing
- Katrijn Gijbels: Methodology, Data curation, Investigation, Writing - Review & Editing
- Pieter Samyn: Data curation, Resources, Writing - Review & Editing
- Valter Carvelli: Validation, Visualization, Writing - Review & Editing
- Mirja Illikainen: Resources, Writing - Review & Editing, Supervision, Funding acquisition
- Paivo Kinnunen: Methodology, Validation, Supervision, Writing - Review & Editing, Funding acquisition

Declaration of competing interest

The authors declare that they have no known competing financial interests or personal relationships that could have appeared to influence the work reported in this paper.

Appendix A

Table A1
Mix proportions (by mass) of the LSG with different citric acid content.

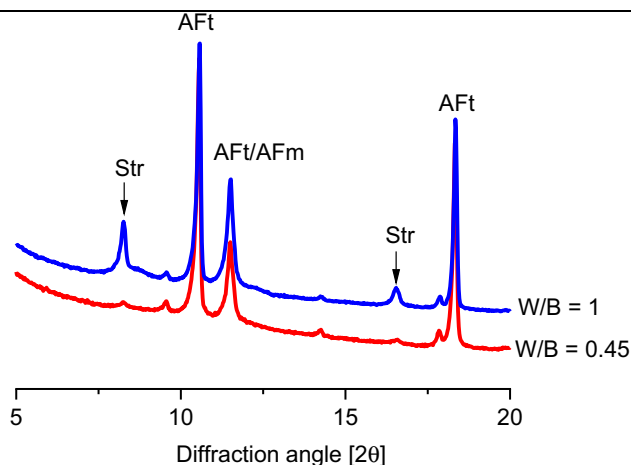| Material	LS	Gypsum	W/B	Citric acid (wt/wt% solution)
LSG-Cit-0.1%	0.7	0.3	0.45	0.1
LSG-Cit-0.5%				0.5
LSG-Cit-1%				1

Fig. A1. The effects of water contain in LSG after 28 days of hydration, in which strätlingite (Str) formed when W/B = 1, whereas the mixture with W/B = 0.45 (reference LSG in this study) did not form strätlingite but C–(A–)S–H gel.
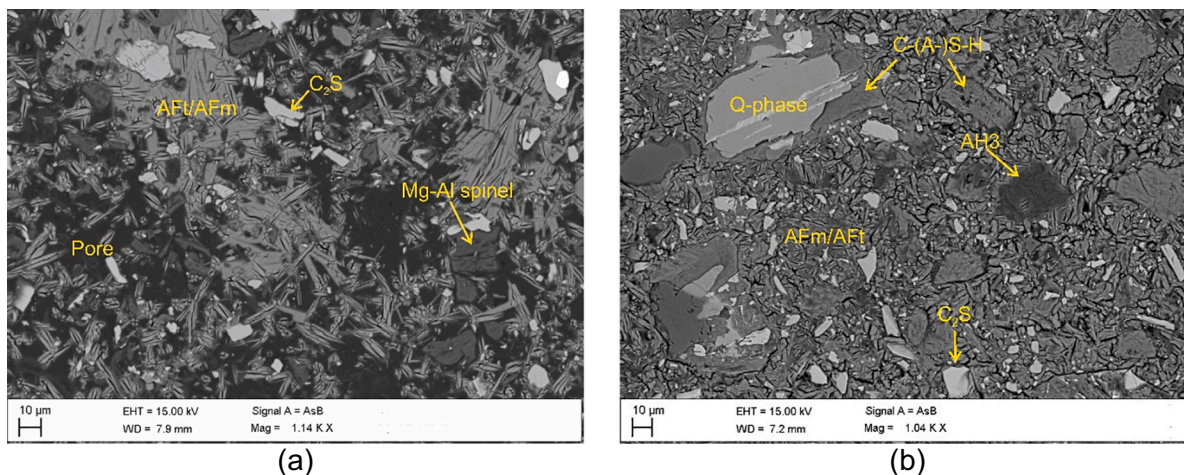

Fig. A2. Microstructure of LSG with (a) W/B = 1 compared to (b) W/B = 0.45 showing that higher water content led to higher degree of hydration in the binder and more void content.
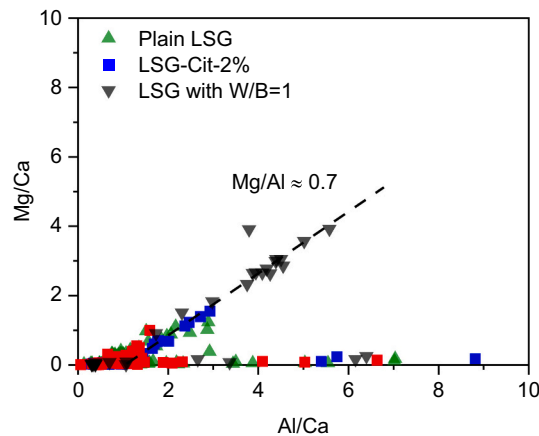
Fig. A3. The Mg/Ca vs. Al/Ca atomic ratio plots obtained from SEM EDS for LSG with W/B = 1 (grey dots) in comparison to plain LSG (green dots) and LSG-Cit-2% (blue dots). This shows the Mg/Al atomic ratio of magnesium aluminate spinel found only in LSG with W/B = 1.
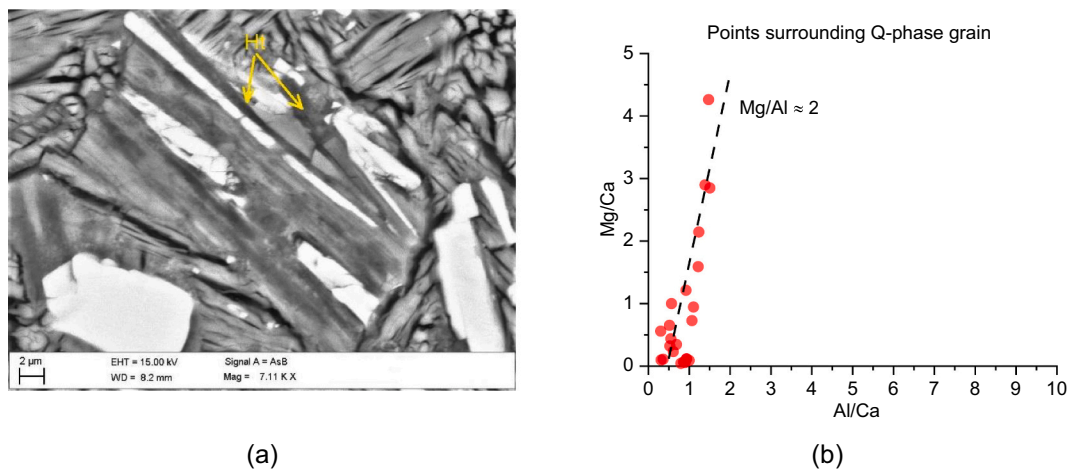

(a)

(b)

Fig. A4. (a) Hydrotalcite formed outside Q-phase grain with (b) Mg/Al atomic ratio around 2.

References

[1] M.C.G. Juenger, F. Winnefeld, J.L. Provis, J.H. Ideker, Advances in alternative cementitious binders, in: Conf. Spec. Cem. Hydration Kinet. Model. Quebec City 2009 CONMOD10 Lausanne 2010 41, 2011, pp. 1232–1243, https://doi.org/10.1016/j.cemconres.2010.11.012.

[2] B. Lothenbach, M. Zajac, Application of thermodynamic modelling to hydrated cements, Cem. Concr. Res. 123 (2019) 105779, https://doi.org/10.1016/j.cemconres.2019.105779.

[3] B. Lothenbach, Thermodynamic equilibrium calculations in cementitious systems, Mater. Struct. 43 (2010) 1413–1433, https://doi.org/10.1617/s11527-010-9592-x.

[4] D. Damidot, B. Lothenbach, D. Herfort, F.P. Glasser, Thermodynamics and cement science, Cem. Concr. Res. 41 (2011) 679–695, https://doi.org/10.1016/j.cemconres.2011.03.018.

[5] B. Lothenbach, D.A. Kulik, T. Matschei, M. Balonis, L. Baquerizo, B. Dilnesa, G.D. Miron, R.J. Myers, Cemdata18: a chemical thermodynamic database for hydrated Portland cements and alkali-activated materials, Cem. Concr. Res. 115 (2019) 472–506, https://doi.org/10.1016/j.cemconres.2018.04.018.

[6] L.J. Parrot, D.C. Killoh, Prediction of cement hydration, in: Br. Ceram. Proc, 1984, pp. 41–53.

[7] W. Kunther, Z. Dai, J. Skibsted, Thermodynamic modeling of hydrated white Portland cement–metakaolin–limestone blends utilizing hydration kinetics from 29Si MAS NMR spectroscopy, Cem. Concr. Res. 86 (2016) 29–41, https://doi.org/10.1016/j.cemconres.2016.04.012.

[8] B. Lothenbach, G. Le Saout, E. Gallucci, K. Scrivener, Influence of limestone on the hydration of Portland cements, Cem. Concr. Res. 38 (2008) 848–860, https://doi.org/10.1016/j.cemconres.2008.01.002.

[9] G. Möschner, B. Lothenbach, R. Figi, R. Kretzschmar, Influence of citric acid on the hydration of Portland cement, Cem. Concr. Res. 39 (2009) 275–282, https://doi.org/10.1016/j.cemconres.2009.01.005.

[10] L. De Windt, A. Bertron, S. Larreur-Cayol, G. Escadeillas, Interactions between hydrated cement paste and organic acids: thermodynamic data and speciation modeling, Cem. Concr. Res. 69 (2015) 25–36, https://doi.org/10.1016/j.cemconres.2014.12.001.

[11] H. Nguyen, P. Kinnunen, K. Gijbels, V. Carvelli, H. Sreenivasan, A.M. Kantola, V.-V. Telkki, W. Schroeyers, M. Illikainen, Ettringite-based binder from ladle slag and gypsum – the effect of citric acid on fresh and hardened state properties, Cem. Concr. Res. 123 (2019) 105800, https://doi.org/10.1016/j.cemconres.2019.105800.

[12] A. Gruskovnjak, B. Lothenbach, F. Winnefeld, R. Figi, S.-C. Ko, M. Adler, U. Mäder, Hydration mechanisms of super sulphated slag cement, Cem. Concr. Res. 38 (2008) 983–992, https://doi.org/10.1016/j.cemconres.2008.03.004.

[13] F. Winnefeld, B. Lothenbach, Hydration of calcium sulfoaluminate cements — experimental findings and thermodynamic modelling, Cem. Concr. Res. 40 (2010) 1239–1247, https://doi.org/10.1016/j.cemconres.2009.08.014.

[14] T. Matschei, B. Lothenbach, F.P. Glasser, The AFm phase in Portland cement, Cem. Concr. Res. 37 (2007) 118–130, https://doi.org/10.1016/j.cemconres.2006.10.010.

[15] L.E. Burris, K.E. Kurtis, Influence of set retarding admixtures on calcium sulfoaluminate cement hydration and property development, Cem. Concr. Res. 104 (2018) 105–113, https://doi.org/10.1016/j.cemconres.2017.11.005.

[16] M. Zajac, J. Skocek, F. Bullerjahn, M. Ben Haha, Effect of retarders on the early hydration of calcium-sulpho-aluminate (CSA) type cements, Cem. Concr. Res. 84 (2016) 62–75, https://doi.org/10.1016/j.cemconres.2016.02.014.

[17] J. Cheung, A. Jeknavorian, L. Roberts, D. Silva, Impact of admixtures on the hydration kinetics of Portland cement, in: Conf. Spec. Cem. Hydration Kinet. Model. Quebec City 2009 CONMOD10 Lausanne 2010 41, 2011, pp. 1289–1309, https://doi.org/10.1016/j.cemconres.2011.03.005.

[18] M. Lanzón, P.A. García-Ruiz, Effect of citric acid on setting inhibition and mechanical properties of gypsum building plasters, Constr. Build. Mater. 28 (2012) 506–511, https://doi.org/10.1016/j.conbuildmat.2011.06.072.

[19] G. Wynn-Jones, R.M. Shelton, M.P. Hofmann, Injectable citrate-modified Portland cement for use in vertebroplasty, J Biomed Mater Res B Appl Biomater 102 (2014) 1799–1808, https://doi.org/10.1002/jbm.b.33160.

[20] NEA Thermochemical Database Project (TDB), (n.d.). http://www.oecd-nea.org/dbtdb/tdbdata/ (accessed July 29, 2019).

[21] L.C. Königsberger, E. Königsberger, P.M. May, G.T. Hefter, Complexation of iron (III) and iron(II) by citrate. Implications for iron speciation in blood plasma, J. Inorg. Biochem. 78 (2000) 175–184, https://doi.org/10.1016/s0162-0134(99)00222-6.

[22] T.E. Zelenina, O.Yu. Zelenin, Complexation of citric and tartaric acids with Na and K ions in aqueous solution, Russ. J. Coord. Chem. 31 (2005) 235–242, https://doi.org/10.1007/s11173-005-0083-5.

[23] R.B. Martin, Citrate binding of Al3+ and Fe3+, J. Inorg. Biochem. 28 (1986) 181–187, https://doi.org/10.1016/0162-0134(86)80081-2.

[24] L. Lutterotti, MAUD: material analysis using diffraction, (n.d.). http://maud.radiographema.eu/ (accessed January 8, 2019).

[25] R. Snellings, L. Machiels, G. Mertens, J. Elsen, Rietveld refinement strategy for quantitative phase analysis of partially amorphous zeolitized tuffaceous rocks, Geol. Belg. 13 (2010) 183–196. https://popups.uliege.be/1374-8505/index.php?id=2923. (Accessed 20 November 2019).

[26] D.L. Bish, S.A. Howard, Quantitative phase analysis using the Rietveld method, J. Appl. Crystallogr. 21 (1988) 86–91, https://doi.org/10.1107/S0021889887009415.

[27] D.A. Kulik, T. Wagner, S.V. Dmytrieva, G. Kosakowski, F.F. Hingerl, K.V. Chudnenko, U.R. Berner, GEM-Selektor geochemical modeling package: revised algorithm and GEMS3K numerical kernel for coupled simulation codes, Comput. Geosci. 17 (2013) 1–24, https://doi.org/10.1007/s10596-012-9310-6.

[28] GEM Software Main Page, (n.d.). http://gems.web.psi.ch/ (accessed November 19, 2019).

[29] F. Goetz-Neunhoeffer, J. Neubauer, P. Schwesig, Mineralogical characteristics of Ettringites synthesized from solutions and suspensions, Cem. Concr. Res. 36 (2006) 65–70, https://doi.org/10.1016/j.cemconres.2004.04.037.

[30] J. Beaudoin, I. Odler, 5 - hydration, setting and hardening of Portland cement, in: P.C. Hewlett, M. Liska (Eds.), Leas Chem. Cem. Concr, Fifth ed., Butterworth-Heinemann, 2019, pp. 157–250, https://doi.org/10.1016/B978-0-08-100773-0.00005-8.

[31] F. Winnefeld, S. Klemm, Influence of citric acid on the hydration kinetics of calcium sulfoaluminate cement, in: 1st Int. Conf. Sulphoaluminate Cem. Mater. Eng. Technol., Wuhan, China, 2013 (pp. 288–208).

[32] Y. Jeong, C.W. Hargis, S.C. Chun, J. Moon, The effect of water and gypsum content on strätlingite formation in calcium sulfoaluminate-belite cement pastes, Constr.

[33] F. Bullerjahn, M. Zajac, M. Ben Haha, K.L. Scrivener, Factors influencing the hydration kinetics of ye'elimite; effect of mayenite, Cem. Concr. Res. 116 (2019) 113–119, https://doi.org/10.1016/j.cemconres.2018.10.026.

[34] D. Herfort, D.E. Macphee, 3 - components in Portland cement clinker and their phase relationships, in: P.C. Hewlett, M. Liska (Eds.), Leas Chem. Cem. Concr, Fifth ed., Butterworth-Heinemann, 2019, pp. 57–86, https://doi.org/10.1016/B978-0-08-100773-0.00003-4.

[35] D. Gastaldi, G. Paul, L. Marchese, S. Irico, E. Boccaleri, S. Mutke, L. Buzzi, F. Canonico, Hydration products in sulfoaluminate cements: evaluation of amorphous phases by XRD/solid-state NMR, Cem. Concr. Res. 90 (2016) 162–173, https://doi.org/10.1016/j.cemconres.2016.05.014.

[36] M. Zajac, J. Skocek, C. Stabler, F. Bullerjahn, M. Ben Haha, Hydration and performance evolution of belite–ye'elimite–ferrite cement, Adv. Cem. Res. 31 (2018) 124–137, https://doi.org/10.1680/jadcr.18.00110.

[37] A. Gruskovnjak, B. Lothenbach, F. Winnefeld, B. Münch, R. Figi, S.-C. Ko, M. Adler, U. Mäder, Quantification of hydration phases in supersulfated cements: review and new approaches, Adv. Cem. Res. 23 (2011) 265–275, https://doi.org/10.1680/adcr.2011.23.6.265.

[38] G. Le Saoût, B. Lothenbach, P. Taquet, H. Fryda, F. Winnefeld, Hydration of calcium aluminate cement blended with anhydrite, Adv. Cem. Res. 30 (2017) 24–36, https://doi.org/10.1680/jadcr.17.00045.

[39] A. Machner, M. Zajac, M. Ben Haha, K.O. Kjellsen, M.R. Geiker, K. De Weerdt, Limitations of the hydrotalcite formation in Portland composite cement pastes containing dolomite and metakaolin, Cem. Concr. Res. 105 (2018) 1–17, https://doi.org/10.1016/j.cemconres.2017.11.007.

[40] F.K. Crundwell, The mechanism of dissolution of forsterite, olivine and minerals of the orthosilicate group, Hydrometallurgy. 150 (2014) 68–82, https://doi.org/10.1016/j.hydromet.2014.09.006.

[41] S. Larreur-Cayol, A. Bertron, G. Escadeillas, Degradation of cement-based materials by various organic acids in agro-industrial waste-waters, Cem. Concr. Res. 41 (2011) 882–892, https://doi.org/10.1016/j.cemconres.2011.04.007.

[42] A.M. Cody, H. Lee, R.D. Cody, P.G. Spry, The effects of chemical environment on the nucleation, growth, and stability of ettringite [Ca3Al(OH)6]2(SO4)3·26H2O, Cem. Concr. Res. 34 (2004) 869–881, https://doi.org/10.1016/j.cemconres.2003.10.023.

[43] G. Zhang, G. Li, Y. Li, Effects of superplasticizers and retarders on the fluidity and strength of sulphoaluminate cement, Constr. Build. Mater. 126 (2016) 44–54, https://doi.org/10.1016/j.conbuildmat.2016.09.019.